

# Anisotropic electron-phonon interaction in the cuprates

T. P. Devereaux\*

*Department of Physics, University of Waterloo, Canada, Ontario N2L 3GI*

T. Cuk<sup>†</sup> and Z.-X. Shen<sup>‡</sup>

*Dept. of Physics, Applied Physics and Stanford Synchrotron Radiation Laboratory, Stanford University, California 94305, USA*

N. Nagaosa<sup>§</sup>

*CREST, Department of Applied Physics, University of Tokyo, Bunkyo-ku, Tokyo 113-8656, Japan*

(Dated: October 31, 2018)

We explore manifestations of electron-phonon coupling on the electron spectral function for two phonon modes in the cuprates exhibiting strong renormalizations with temperature and doping. Applying simple symmetry considerations and kinematic constraints, we find that the out-of-plane, out-of-phase O buckling mode ( $B_{1g}$ ) involves small momentum transfers and couples strongly to electronic states near the anti-node while the in-plane Cu-O breathing modes involve large momentum transfers and couples strongly to nodal electronic states. Band renormalization effects are found to be strongest in the superconducting state near the anti-node, in full agreement with angle-resolved photoemission spectroscopy (ARPES) data.

PACS numbers:

The electron-phonon interaction in metals is generally considered to be isotropic. Recent developments in the cuprates however raises important questions about this assumption. The renewed interest stems from the observation of bosonic band renormalization effects in a wide range of p-type materials[1]. This effect is found to be dramatically enhanced below  $T_c$  near the  $(\pi, 0)$  regions in the Brillouin zone (BZ)[2]. Such a momentum and temperature dependence appears to support the idea that the bosonic renormalizations in p-type materials is due to a coupling of the electrons to the 41 meV spin resonance mode that appears below  $T_c$ [3, 4].

On the other hand, it has been argued that the bosonic renormalization effect may be reinterpreted as a result of a coupling to the half-breathing in-plane Cu-O bond-stretching phonon for nodal directions[5] and the out-of-plane out-of-phase O buckling  $B_{1g}$  phonon for anti-nodal directions[6]. This re-interpretation has the clear advantage over the spin resonance in that it naturally explains why the band renormalization effect is observed under three circumstances: 1) in materials where no spin mode has been detected, 2) in the normal state, and 3) in the deeply overdoped region where the spin mode is neither expected nor observed. However this interpretation also requires that the electron-phonon interaction to be highly anisotropic and its impact on the electrons to be strongly enhanced in the superconducting state. This is something one does not expect a priori.

This paper investigates the anisotropy of the electron-phonon interaction of two known phonons - the half-breathing mode and the  $B_{1g}$  buckling mode - formulated within the same framework as that used to explain phonon lineshape changes observed via Raman and neutron measurements[4, 7, 8, 9]. We find that the electron-

phonon interactions to be very anisotropic as a consequence of the following four properties of the cuprates: 1) the symmetry of the phonon polarizations and electronic orbitals involved leading to highly anisotropic electron-phonon coupling matrix elements  $g(k, q)$ ; 2) the kinematic constraint related to the anisotropy of the electronic band structure and the van Hove singularity (VHS); 3) the d-wave superconducting gap, and 4) the near degeneracy of energy scales of the  $B_{1g}$  phonon, the superconducting gap, and the VHS. Taking into account these and thermal effects we can naturally explain the observed momentum and temperature dependence of the data, leading to unified understanding of band renormalizations.

Our starting point is the tight-binding three-band Hamiltonian modified by  $B_{1g}$  buckling vibrations as considered in Ref. [10] and in-plane breathing vibrations as considered in Ref. [11]:

$$\begin{aligned}
 H = & \sum_{\mathbf{n}, \sigma} \epsilon_{Cu} b_{\mathbf{n}, \sigma}^\dagger b_{\mathbf{n}, \sigma} \\
 & + \sum_{\mathbf{n}, \delta, \sigma} \{ \epsilon_O + eE_z u_\delta^O(\mathbf{n}) \} a_{\mathbf{n}, \delta, \sigma}^\dagger a_{\mathbf{n}, \delta, \sigma} \\
 & + \sum_{\mathbf{n}, \delta, \sigma} P_\delta [t - Q_\delta g_{dp} u_\delta^O(\mathbf{n})] (b_{\mathbf{n}, \sigma}^\dagger a_{\mathbf{n}, \delta, \sigma} + h.c.) \\
 & + t' \sum_{\mathbf{n}, \delta, \delta'} P_{\delta, \delta'} (a_{\mathbf{n}, \delta}^\dagger a_{\mathbf{n}, \delta', \sigma} + h.c)
 \end{aligned} \tag{1}$$

with Cu-O hopping amplitude  $t$ , O-O amplitude  $t'$ , and  $\epsilon_{d,p}$  denoting the Cu and O site energies, respectively. Here  $a_{\alpha=x,y}, a_{\alpha=x,y}^\dagger$  ( $b, b^\dagger$ ) annihilates, creates an electron in the  $O_\alpha$  (Cu) orbital, respectively. The overlap factors  $Q_\delta, P_\delta$ , and  $P_{\delta, \delta'}$  are given in our notation as  $Q_{\pm x} = Q_{\pm y} = \pm 1; P_{\pm x} = -P_{\pm y} = \pm 1; P_{\pm x, \pm y} = 1 = -P_{\mp x, \pm y}$ .

For the half-breathing mode we consider only couplings  $g_{dp} = q_0 t$  (with  $1/q_0$  a length scale) arising from modulation of the covalent hopping amplitude  $t$ [11, 12]. For the  $B_{1g}$  mode a coupling to linear order in the atomic displacements arises from a local c-axis oriented crystal field  $E_z$  which breaks the mirror plane symmetry of the Cu-O plane[10].

The symmetry of the  $p, d$  wavefunctions of the Cu-O plane is embedded in the amplitudes  $\phi$  of the tight-binding wavefunctions forming the anti-bonding band with energy dispersion  $\epsilon(\mathbf{k})$  arising from Eq. 1. Specifically the transformation is determined by the projected part of the tight-binding wavefunctions  $b_{\mathbf{k},\sigma} = \phi_b(\mathbf{k})d_{\mathbf{k},\sigma}$  and  $a_{\alpha,k,\sigma} = \phi_\alpha(\mathbf{k})d_{\mathbf{k},\sigma}$ ,

$$\phi_b(\mathbf{k}) = \frac{1}{N(\mathbf{k})} [\epsilon^2(\mathbf{k}) - t'^2(\mathbf{k})], \quad (2)$$

$$\phi_{x,y}(\mathbf{k}) = \frac{\mp i}{N(\mathbf{k})} [\epsilon(\mathbf{k})t_{x,y}(\mathbf{k}) - t'(\mathbf{k})t_{y,x}(\mathbf{k})], \quad (3)$$

with  $N^2(\mathbf{k}) = [\epsilon^2(\mathbf{k}) - t'^2(\mathbf{k})]^2 + [\epsilon(\mathbf{k})t_x(\mathbf{k}) - t'(\mathbf{k})t_y(\mathbf{k})]^2 + [\epsilon(\mathbf{k})t_y(\mathbf{k}) - t'(\mathbf{k})t_x(\mathbf{k})]^2$ ,  $t_\alpha(\mathbf{k}) = 2t \sin(k_\alpha a/2)$ , and  $t'(\mathbf{k}) = 4t \sin(k_x a/2) \sin(k_y a/2)$ .

The projected wavefunctions act in conjunction with the phonon eigenvectors to determine the full symmetry of the electron-phonon coupling:  $H_{el-ph} = \frac{1}{\sqrt{N}} \sum_{\mathbf{k},\mathbf{q},\sigma,\mu} g_\mu(\mathbf{k},\mathbf{q}) c_{\mathbf{k},\sigma}^\dagger c_{\mathbf{k}+\mathbf{q},\sigma} [a_{\mu,\mathbf{q}}^\dagger + a_{\mu,-\mathbf{q}}]$ . Neglecting the motion of the heavier Cu atoms compared to O in the phonon eigenvectors the form of the respective couplings can be compactly written as

$$g_{B_{1g}}(\mathbf{k}, \mathbf{q}) = eE_z \sqrt{\frac{\hbar}{4M_O M(\mathbf{q}) \Omega_{B_{1g}}}} \quad (4)$$

$$\times \{ \phi_x(\mathbf{k})\phi_x(\mathbf{k}') \cos(q_y a/2) - \phi_y(\mathbf{k})\phi_y(\mathbf{k}') \cos(q_x a/2) \}$$

$$g_{br}(\mathbf{k}, \mathbf{q}) = g_{dp} \sqrt{\frac{\hbar}{2M_O \Omega_{br}}} \sum_{\alpha=x,y} \quad (5)$$

$$\times \{ \phi_b(\mathbf{k}')\phi_\alpha(\mathbf{k}) \cos(k'_\alpha a/2) - \phi_b(\mathbf{k})\phi_\alpha(\mathbf{k}') \cos(k_\alpha a/2) \},$$

with  $M(\mathbf{q}) = [\cos^2(q_x a/2) + \cos^2(q_y a/2)]/2$  and  $\mathbf{k}' = \mathbf{k} - \mathbf{q}$ . A simple consequence of symmetry can be observed at small momentum transfers  $\mathbf{q}$  where  $g_{B_{1g}}(\mathbf{k}, \mathbf{q} = \mathbf{0}) \sim \cos(k_x a) - \cos(k_y a)$ , while  $g_{br} \sim \sin(qa)$  for any  $\mathbf{k}$ . Yet for large momentum transfer  $\mathbf{q} = (\pi/a, \pi/a)$ ,  $g_{B_{1g}}$  vanishes for all  $\mathbf{k}$  while  $g_{br}$  has its maximum for  $\mathbf{k}$  located on the nodal points of the Fermi surface. This  $q$ -dependence has been the focus before in context with a  $d_{x^2-y^2}$  pairing mechanism[13, 14], but the dependence on fermionic wavevector  $\mathbf{k}$  has usually been overlooked. It is exactly this fermionic dependence which we feel is crucially needed to interpret ARPES data.

These features of each coupling constant can be seen in Fig 1 which plots  $|g(\mathbf{k}, \mathbf{q})|^2$  as a function of phonon scattered momentum  $\mathbf{q}$  connecting initial  $\mathbf{k}$  and final

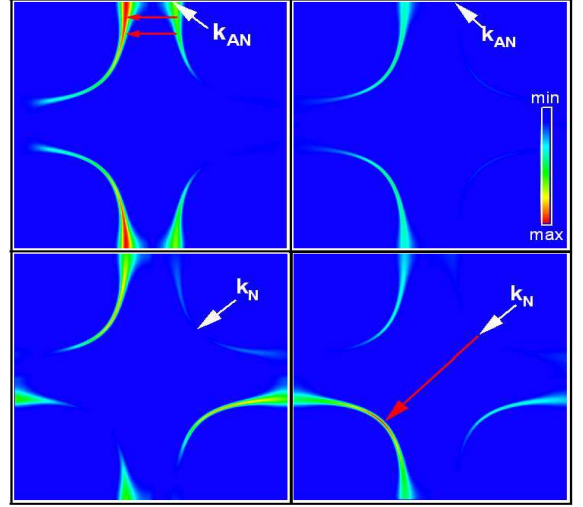


FIG. 1: Plots of the electron-phonon coupling  $|g(\mathbf{k}, \mathbf{q})|^2$  for initial  $\mathbf{k}$  and scattered  $\mathbf{k}' = \mathbf{k} - \mathbf{q}$  states on the Fermi surface for the buckling mode (left panels) and breathing mode (right panels) for initial fermion  $\mathbf{k}$  at an anti-nodal (top panels) and nodal (bottom panels) point on the Fermi surface, as indicated by the arrows. The red/blue color indicates the maximum/minimum of the el-ph coupling vertex in the BZ for each phonon.

$\mathbf{k}' = \mathbf{k} - \mathbf{q}$  fermion states both on the Fermi surface. Here we have adopted a five-parameter fit to the band structure used previously for optimally doped Bi-2212[3]. For an anti-nodal initial fermion  $\mathbf{k}_{AN}$ , the coupling to the  $B_{1g}$  phonon is largest for  $2\mathbf{k}_F$  scattering to an anti-nodal final state. The coupling to the breathing mode is much weaker overall, and is especially weak for small  $\mathbf{q}$  and mostly connects to fermion final states at larger  $\mathbf{q}$ . For a nodal fermion initial state  $\mathbf{k}_N$ , the  $B_{1g}$  coupling is suppressed for small  $\mathbf{q}$  and has a weak maximum towards anti-nodal final states, while the breathing mode attains its largest value for scattering to other nodal states, particularly to state  $-\mathbf{k}_N$ .

In Fig. 2 we show effective couplings  $\lambda_{\mathbf{k}}$  (summed over all  $\mathbf{q}$ ) for  $\mathbf{k}$  points in the first quadrant of the BZ in the normal state[14]. Here we have used the value of the electric field  $eE_z = 1.85 \text{ eV}/\text{\AA}$  consistent with Raman scattering measurements of the  $B_{1g}$  phonon and buckling of the Cu-O plane in YBaCuO, and have taken  $q_0 t = 2\sqrt{2}eE_z$  as a representative value for the coupling to the breathing mode. These values lead to net couplings similar to that obtained from LDA calculations[14]. As a result of the anisotropy of the coupling constant, large enhancements of the coupling near the anti-node for the  $B_{1g}$  phonon, and nodal directions for the breathing phonon mode are observed, respectively, which are an order of magnitude larger than the average  $\lambda$ 's.

We now turn to the spectral function. The dynamic nature of the coupling is governed by the energy scales of the band structure, phonon frequencies, and super-

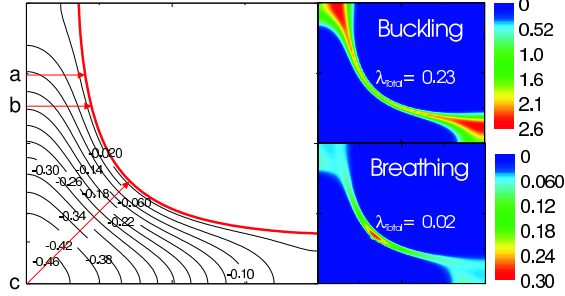


FIG. 2: Plots of the electron-phonon coupling  $\lambda_k$  in the first quadrant of the BZ for the buckling mode (right top panel) and breathing mode (right bottom panel). The color scale is shown on the right for each phonon. The left panel shows energy contours for the band structure used[3].

conducting gap energy, and are manifest in features of the Nambu-Eliashberg electron-phonon self-energy[15]:  $\hat{\Sigma}(\mathbf{k}, i\omega_m) = i\omega_m(1 - Z(\mathbf{k}, i\omega_m))\hat{\tau}_0 + \chi(\mathbf{k}, i\omega_m)\hat{\tau}_3 + \Phi(\mathbf{k}, i\omega_m)\hat{\tau}_1$  with

$$\hat{\Sigma}(\mathbf{k}, i\omega_m) = \frac{1}{\beta N} \sum_{\mathbf{p}, \mu, m} g_\mu(\mathbf{k}, \mathbf{p}-\mathbf{k}) g_\mu(\mathbf{p}, \mathbf{k}-\mathbf{p}) \times D_\mu^0(\mathbf{k}-\mathbf{p}, i\omega_m - i\omega_n) \hat{\tau}_3 \hat{G}^0(\mathbf{p}, i\omega_m) \hat{\tau}_3, \quad (6)$$

with  $\hat{G}^0(\mathbf{p}, i\omega_m) = \frac{i\omega_m \tau_0 + \epsilon(\mathbf{p})\hat{\tau}_3 + \Delta(\mathbf{p})\hat{\tau}_1}{(i\omega_m)^2 - E^2(\mathbf{p})}$  and  $E^2(\mathbf{k}) = \epsilon^2(\mathbf{k}) + \Delta^2(\mathbf{k})$ , with  $\hat{\tau}_{i=0\dots 3}$  are Pauli matrices. We take  $\Delta(\mathbf{k}) = \Delta_0[\cos(k_x a) - \cos(k_y a)]/2$  with  $\Delta_0 = 35\text{meV}$ . The bare phonon propagators are taken as  $D_\mu^0(\mathbf{q}, i\Omega_\nu) = \frac{1}{2} \left[ \frac{1}{i\Omega_\nu - \Omega_\mu} - \frac{1}{i\Omega_\nu + \Omega_\mu} \right]$ . Here we take dispersionless optical phonons  $\hbar\Omega_{B_{1g}, br} = 36, 70\text{meV}$ , respectively.

The spectral function  $A(\mathbf{k}, \omega) = -\frac{1}{\pi} \text{Im}G_{11}(k, i\omega \rightarrow \omega + i\delta)$  is determined from Eq. 6 with  $\hat{G}(k, i\omega_m) = [\hat{\tau}_0 i\omega_m Z(\mathbf{k}, i\omega_m) - (\epsilon(\mathbf{k}) + \chi(\mathbf{k}, i\omega_m))\hat{\tau}_3 - \Phi(\mathbf{k}, i\omega_m)\hat{\tau}_1]^{-1}$  and the coupling constants given by Eq. 4-5. Here we consider three different cuts: along the nodal direction ( $k_x = k_y$ , denoted by  $c$ ), and two cuts parallel to the BZ face ( $k_y = 0.75\pi/a$ ,  $b$ ) and ( $k_y = 0.64\pi/a$ ,  $a$ ) where bilayer effects are not severe[6], as indicated in Fig. 2.

Our results for the three cut directions are shown in Fig 3 for the normal ( $T = 110\text{K}$ ) and superconducting ( $T = 10\text{K}$ ) states. One can only observe very weak kink features in the normal state, but a much more pronounced kink at 70 meV in the superconducting state is observed for all the cuts, in excellent agreement with the data[6], shown also in Fig. 3. The dramatic temperature dependence stems from a substantial change in the electronic occupation distribution and the opening of the superconducting gap. In the normal state, the phonon self energy is a Fermi function at 110K centered at the phonon frequency, which results in a thermal broadening of  $4.4k_B T$  or 50meV, comparable to phonon frequencies. At 10K in the superconducting state, on the other hand, the phonon self energy is sharply defined due to

the step-function-like Fermi function and a singularity in the superconducting density of states. These factors, together with the experimental difficulty in detecting a weak effect, conspire to leave the false impression that the bosonic mode merges below  $T_c$ , as invoked by the spin resonance scenario[3].

In the superconducting state, the data and the theory exhibit a rich variety of signatures in the electron-phonon coupling: cut  $a$  exhibits the strongest signatures of coupling, showing an Einstein like break up into a band that follows the phonon dispersion, and one that follows the electronic one; in cut  $b$ , a weaker signature of coupling manifests itself in an  $s$ -like renormalization of the bare band that traces the real part of the phonon self-energy; and in cut  $c$ , where the coupling to the  $B_{1g}$  phonon is weakest, the electron-phonon coupling manifests itself as a change in the velocity of the band. The agreement is very good, even for the large change in the electron-phonon coupling seen between cuts  $a$  and  $b$ , separated by only 1/10th of the BZ.

We now discuss the reason for the strong anisotropy as a result of a concurrence of symmetries, band structure,  $d$ -wave energy gap, and energy scales in the electron-phonon problem. In the normal state, weak kinks are observed at both phonon frequencies, but more pronounced at 70 meV for cut  $c$  and at 36 meV for cut  $a$ , as expected from the anisotropic couplings shown in Fig. 1. However this is also a consequence of the energy scales of the phonon modes and the bottom of electronic band along the cut direction as shown in Fig. 2. Further towards the anti-node, another interesting effect occurs. As one considers cuts closer to the BZ axis, the bottom of the band along the cut rises in energy and the breathing phonon mode lies below the bottom of the band for ( $k_x = 0, k_y > 0.82\pi/a$ ) and so the kink feature for this mode disappears. This is the usual effect of a Fano redistribution of spectral weight when a discrete excitation lies either within or outside of the band continuum[16]. This thus can be used to open "windows" to examine the coupling of electrons to discrete modes in general. Taken together, this naturally explains why the normal state nodal kink is near 70 meV[5] while the anti-nodal kink is near 40 meV[2, 6].

In the superconducting state the bare band renormalizes downward in energy due to the opening of the gap and gives the strongest effect for the anti-nodal region where the gap is of the order of the saddle point energy. This also gives the appearance of an increase of bandwidth. The  $B_{1g}$  coupling becomes dramatically enhanced by the opening of the gap at a frequency close to the frequency of the phonon itself, and leads to the dramatic renormalization of the phonon observed in Raman and neutron measurements[7]. Yet the breathing coupling does not vary dramatically as the large gap region is not weighted as heavily by the coupling constant. As a consequence, the  $B_{1g}$  mode dominates and clear kinks in

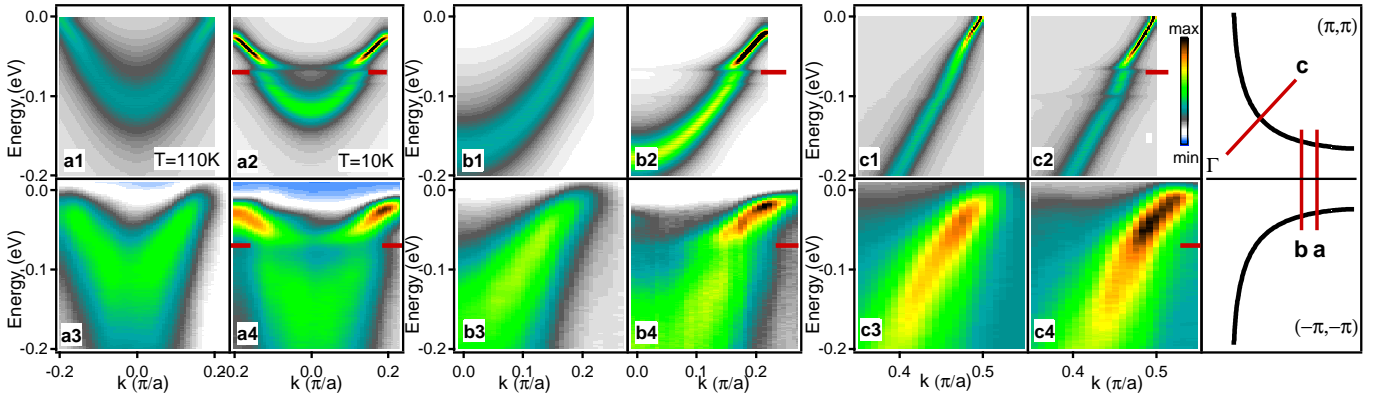


FIG. 3: Image plots of the calculated spectral functions in the normal (a1,b1,c1) and superconducting (a2,b2,c2) states compared to the spectral functions in the normal (a3,b3,c3) and superconducting (a4,b4,c4) states measured in  $\text{Bi}_2\text{Sr}_2\text{Ca}_{0.92}\text{Y}_{0.08}\text{Cu}_2\text{O}_{8+\delta}$  (Bi-2212)[6] for momentum cuts  $a,b,c$  shown in the right-most panel and in Figure 2. The same color scale is used for the normal/superconducting pairs within each cut, but the scaling for the data and the calculation are separate. The red markers indicate 70meV in the superconducting state.

the data are revealed at around 70 meV - the  $B_{1g}$  energy plus the gap. Indeed a much weaker kink at 105 meV from the breathing phonon shows at higher energies for the nodal cut but this kink becomes weaker away from nodal directions as the coupling and the band bottom along the cut moves below the phonon frequency so that the “energy window” closes.

Our work is formulated in the context of band structure and one phonon process. Fig. 3 indicates that such an approach catches the key features of the band renormalization effects due to optical phonons in the 35-70 meV range, something unexpected a priori given the strong correlation effects in these materials. Additional broadening in the data of Fig. 3 is likely a manifestation of the Coulomb correlation over a broad energy range. A next step is to incorporate the correlation effect, vertex correction, and possible non-linear phonon effects, especially as we push towards underdoped regime. These are challenges ahead. On the other hand, the current approach allows us to study the doping trend in the overdoped regime.

In summary, contrary to usual opinion of the role of anisotropy in electron-phonon coupling, the interplay of specific coupling mechanisms of electrons to the buckling and breathing phonons give a natural interpretation to the bosonic renormalization effects seen in ARPES in both the normal and superconducting states, and provides a framework to understand renormalizations as a function of doping.

<sup>§</sup> Electronic address: nagaosa@appi.t.u-tokyo.ac.jp; URL: <http://appi.t.u-tokyo.ac.jp/index-e.htm>

- [1] A. Damszelli, Z. Hussain and Z. -X. Shen, Rev. Mod. Phys. **75**, 473 (2003), and references therein.
- [2] A. Gromko *et al.*, Phys. Rev. B **68**, 174520 (2003); T. Sato *et al.*, Phys. Rev. Lett. **91**, 157003 (2003); T. K. Kim *et al.*, Phys. Rev. Lett. **91**, 167002 (2003).
- [3] M. R. Norman *et al.*, Phys. Rev. B **64**, 184508 (2001). M. Eschrig and M. R. Norman, Phys. Rev. Lett. **85**, 3261 (2000); Phys. Rev. B **67**, 144503 (2003); A. V. Chubukov and M. R. Norman, cond-mat/0402304.
- [4] H.-Y. Kee *et al.*, Phys. Rev. Lett. **88**, 257002 (2002); Ar. Abanov *et al.*, Phys. Rev. Lett. **89**, 177002 (2002).
- [5] A. Lanzara *et al.*, Nature **412**, 510 (2001); Z.-X. Shen *et al.*, Phil. Mag. B **82**, 1349 (2002); X. J. Zhou *et al.*, Nature **423**, 398 (2003).
- [6] T. Cuk *et al.*, preprint.
- [7] B. Friedl *et al.*, Phys. Rev. Lett. **65**, 915 (1990); N. Pyka *et al.*, Phys. Rev. Lett. **70**, 1457 (1993); D. Reznik *et al.*, Phys. Rev. Lett. **75**, 2396 (1995).
- [8] S. L. Chaplot *et al.*, Phys. Rev. B **52**, 7230 (1995); R.J. McQueeney *et al.*, Phys. Rev. Lett. **82**, 628 (1999); **87**, 077001 (2001); J.-H. Chung *et al.*, Phys. Rev. B **67**, 014517 (2003); S. Sugai *et al.*, Phys. Rev. B **68**, 184504 (2003).
- [9] M. Opel *et al.*, Phys. Rev. B **60**, 9836 (1999).
- [10] T. P. Devereaux, A. Virosztek, and A. Zawadowski Phys. Rev. B **59**, 14618 (1999); **51**, 505 (1995).
- [11] S. Barišić, Phys. Rev. B **5**, 932 (1972).
- [12] The coupling  $g_d$  arising from modulation of Cu site energies leads to a coupling which only depends on momentum transfers on not on fermion momentum[11].
- [13] D.J. Scalapino, J. Phys. Chem. Solids **56**, 1669 (1995); A. Nazarenko and E. Dagotto, Phys. Rev. B **53**, 2987 (1996); T. S. Nunner, J. Schmalian and K. H. Bennemann, Phys. Rev. B **59**, 8859 (1999).
- [14] O. Jepsen *et al.*, J. Phys. Chem. Solids **59**, 1718 (1998).
- [15] A. W. Sandvik *et al.*, cond-mat/0309171.
- [16] U. Fano, Phys. Rev. **124**, 1866 (1961).
- [17] ARPES data were collected at SSRL which is operated by DOE under contract DE-AC03-76SF00515. T.P.D. would

\* Electronic address: tpd@lorax.uwaterloo.ca; URL: <http://www.sciborg.uwaterloo.ca/~tpd/>

<sup>†</sup> Electronic address: tanjacuk@stanford.edu

<sup>‡</sup> Electronic address: zxshen@stanford.edu; URL: <http://arpes.stanford.edu/>

like to acknowledge support from NSERC, PREA and the A. von Humboldt Foundation. The Stanford work is also

supported by NSF grant DMR-0304981 and ONR grant N00014-01-1-0048.